

# SURVIVAL AND INVASION DYNAMICS IN CELL POPULATIONS: AN ANALYTICAL FRAMEWORK FOR THRESHOLD BEHAVIOUR IN NONLINEAR AGE-STRUCTURED MODELS

STÉPHANIE M. C. ABO\* AND RUTH E. BAKER\*

**Abstract.** Cell populations invade through a combination of proliferation and motility. Proliferation depends on the internal timing of cell division: how long cells take to complete the cell cycle. This timing varies substantially within (and across) cell types, creating age structure where cells at different times since their last division have different propensities to divide. Classical mathematical models of cell spreading treat division as memoryless and predict exponential cell-cycle-time distributions. Lineage tracing, by contrast, reveals peaked, gamma-like distributions that indicate a maturation delay leading to a fertility window. This gap motivates a modelling framework that incorporates age-dependent cell division rates while retaining analytical tractability.

We address this through a moment-hierarchy framework that tracks time since cell division, with age resetting to zero at division. The framework yields explicit formulae for steady-state age distributions, cell-cycle-time distributions, and invasion speeds. For age-independent rates, we recover classical Fisher–KPP. Three fundamental principles emerge. First, age structure systematically reduces a population’s carrying capacity and narrows the viable parameter range for positive steady states. Second, classical linear theory overestimates invasion speeds; the true minimal speed is slower when division is age-dependent. Third, the parameter condition for population survival is identical to the condition for a positive invasion speed.

**Relevance to Life Sciences.** Our study addresses a fundamental question in wound healing, tissue regeneration, and tumour invasion: how the timing of cell division regulates whether populations can persist and how fast they spread? By deriving explicit formulae for cell-cycle-time distributions, we link single-cell measurements of division timing to population-level outcomes—thresholds in division and death rates that determine population persistence and the rate of invasion. These formulae enable direct parameter estimation from lineage-tracing data, demonstrated by fitting division-time measurements from cells under control and perturbed conditions. The results show that interventions that prolong the cell cycle shift populations toward extinction. The relationship between division timing and invasion speed provides a mechanistic basis for interpreting competitive outcomes in collective cell migration and tissue dynamics.

**Mathematical Content.** We formulate an age-structured transport-renewal equation for a motile and proliferating cell population, where cell age tracks time since last division and resets to zero upon division. Cell division and death are modelled as distinct processes, each dependent on cell age and population density. We derive a generalised moment system that connects the total population to its age-weighted moments. This reduction preserves the essential structure of the model while providing a finite-dimensional, tractable system. We classify models by their rate functions—constant, exponentially decaying, or gamma-type—representing age-homogeneous, early-biased, and delayed division. For each case, this framework yields explicit expressions for the population survival condition, the steady-state age and cell-cycle-time distributions, and the minimal invasion speed, all derived without closure approximations.

**Key words.** Cell cycle dynamics, division timing, structured populations, Fisher–KPP equation, travelling waves, integro-differential equations, survival conditions.

**MSC codes.** 92D25, 35Q92, 35C07, 35R09

**1. Introduction.** The coordinated behaviour of motile and proliferative cells is fundamental to embryonic development, tissue regeneration, wound healing, and tumour invasion. In such processes, spatial expansion occurs through *collective cell invasion*, where cells move as cohesive groups with mechanical and biochemical coupling [1]. These dynamics depend on both external cues (adhesion, confinement) and internal cell-cycle state [2, 3, 4]. The cell cycle imposes a necessary maturation delay before division can occur, acting as a key biological constraint. The progression time through the cell cycle, measured as the intermitotic time (IMT), exhibits marked heterogeneity in experimental data [5, 6]. High-resolution lineage tracing reveals IMT distributions that are typically gamma-like, with defined peaks and right skew, rather than exponential as assumed in memoryless birth models [7] (Figure 1(a)). This discrepancy indicates that models assuming constant division rates across the cell cycle do not account for essential biological regulation.

Non-exponential division timing has motivated structured modelling approaches that account for how internal states constrain and delay cell division (Figure 1(b)). These approaches introduce continuous variables representing internal timing [9, 10, 11, 12]. *Cell age* can denote chronological age, phase duration, or generational time; age-structured partial differential equations (PDEs) provide a general formalism accommodating this variability. Here, we focus on cell age as time since last division—a biologically grounded assumption aligning with experimental measurement of cell-cycle times. This simplification aggregates sub-stages while providing a meaningful foundation for future extensions incorporating finer-grained structure.

Classical mathematical models of population spread, such as the Fisher–KPP (Fisher–Kolmogorov–

---

\*Mathematical Institute, University of Oxford, UK ([stephanie.abo@maths.ox.ac.uk](mailto:stephanie.abo@maths.ox.ac.uk)).

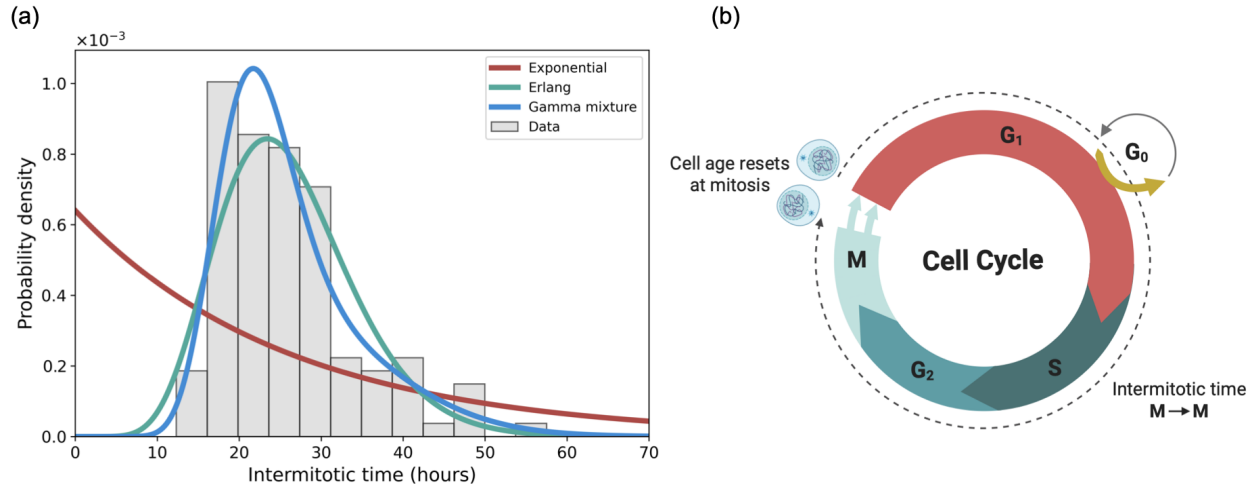


FIG. 1. (a) Distribution of intermitotic times (IMTs) from lineage-tracing data (grey bars) with fitted exponential (red), Erlang (green), and gamma mixture (blue) models. (b) Schematic of the cell cycle. Cells progress through four main phases: Gap 1 (G<sub>1</sub>, growth and preparation for DNA synthesis), Synthesis (S, DNA replication), Gap 2 (G<sub>2</sub>, preparation for mitosis), and Mitosis (M, cell division; here mitosis and cell division are used interchangeably). In our model, cell age (defined as time since last division) resets to zero upon mitosis, providing a coarse-grained representation of cell-cycle progression. The intermitotic time (IMT) is measured from one mitosis to the next (M→M). Experimental IMT data reproduced with permission, courtesy of Richard L. Mort (Lancaster University) and Matthew J. Ford (University of Cambridge), provided by Christian A. Yates (University of Bath). Cell-cycle stages adapted from [8] (BioRender).

Petrovsky–Piskunov) equation, assume cells divide at a constant rate independent of time since division. These models do not account for the finite time required to complete the cell cycle, which affects division-time distributions and the capacity of populations to persist or invade. Age-structured models address this gap by tracking the joint evolution of density and internal time. The foundational works of McKendrick [13] and von Foerster [14] formalised transport equations where individuals progress deterministically through age. In the simplest linear setting, populations grow exponentially and approach stable age distributions. Gurtin and MacCamy [15, 16] extended this to include density dependence, spatial diffusion, and biologically motivated division kernels where division rates peak at intermediate ages. Their formulation combined division and death within a single loss term, with age dependence appearing only in the boundary condition. This simplified the mathematics but limited the capacity to distinguish how ageing, division, and death separately influence dynamics.

Spatial theory advanced with the work of Al-Omari and Gourley [17], who established the existence of travelling waves in age-structured reaction-diffusion models. Gourley [18] proved linear stability of travelling fronts, and Li, Mei, and Wong [19] extended this to nonlinear stability, though initially restricted to small maturation delays. Mei and Wong [20] later proved nonlinear stability for arbitrarily large delays. In applied contexts, structured PDEs have been used to model cell-cycle regulation in proliferating tissues [21] and to connect multi-stage stochastic frameworks with continuous age-structured formalisms [10]. More recently, Pang and Pardoux [22] established formal connections between stochastic individual-based models, renewal equations, and age-structured PDEs. Despite these advances, most nonlinear age-structured PDEs remain analytically intractable. Explicit characterisations of steady states, division-time distributions, and invasion speeds remain rare, limiting the ability to derive interpretable predictions from such models.

We develop an analytical framework for collective cell invasion that links single-cell division timing to population survival and invasion. Models are classified by their rate functions—constant, exponentially decaying, or gamma-like. Integration with respect to age yields a set of integro-differential equations where age structure enters through weighted integrals. This finite integro-differential formulation can be analysed directly, without closure approximations. Division and death are treated as separate processes, each dependent on cell age and local density. We treat non-spatial and spatial dynamics. In the non-spatial setting, we obtain explicit formulae for steady-state age distributions, cell-cycle-time distributions, and the parameter

conditions for population survival. In the spatial setting, we derive expressions for the minimal wave speed and recover the classical Fisher–KPP limit when division and death are age-independent. To our knowledge, this is the first deterministic analysis within this class of nonlinear age-structured PDEs to provide explicit cell-cycle-time distributions together with survival conditions and invasion criteria. It addresses a gap previously approached only through stochastic or discrete-time models [7, 23]. We show that the shape of the division kernel controls both population survival and invasion speed. Biologically, the results account for the gamma-shaped division-time distributions observed in lineage-tracing data and demonstrate how longer division times slow invasion. The framework links measurable quantities to the underlying division and death mechanisms.

The paper is structured as follows. Section 2 introduces the age-structured model and derives the moment-hierarchy reduction. Section 3 analyses non-spatial dynamics and establishes survival thresholds that depend systematically on division kernel shape. Sections 4–5 characterise steady-state age distributions and cell-cycle-time distributions. Section 6 establishes minimal wave speeds for spatial models and shows that classical linear theory overestimates invasion rates when division is age-dependent. Section 7 discusses biological implications and experimental validation. Our approach builds on the work of Gurtin and MacCamy [15, 16] but diverges by separating division and death explicitly, retaining age-dependence in both loss terms, and deriving analytical results without closure assumptions.

**2. Model framework.** We model a motile and proliferative cell population, where cell age tracks time since last division. Let  $u(a, x, t)$  represent the density of cells of age  $a \geq 0$  at position  $x \in \Omega \subseteq \mathbb{R}^d$  and time  $t \geq 0$ , with total population

$$(2.1) \quad P(x, t) = \int_0^\infty u(a, x, t) da.$$

Cells age at unit rate, move diffusively with coefficient  $\kappa \geq 0$ , and are removed by death at rate  $\mu(a, P) \geq 0$  or division at rate  $\beta(a, P) \geq 0$ . Upon division, two daughter cells enter at age zero, giving the transport-renewal system

$$(2.2) \quad \partial_t u + \partial_a u = \kappa \Delta u - [\mu(a, P(x, t)) + \beta(a, P(x, t))] u,$$

$$(2.3) \quad u(0, x, t) = 2 \int_0^\infty \beta(a, P(x, t)) u(a, x, t) da.$$

The boundary condition (2.3) represents the influx of newborn cells. Initial data are  $u(a, x, 0) = u_0(a, x) \geq 0$ . For bounded  $\Omega$ , we impose no-flux boundary conditions (confined tissue). For  $\Omega = \mathbb{R}^d$ , one may assume decay as  $|x| \rightarrow \infty$  (unbounded spread).

The model captures two mechanisms. First, division and death rates depend on cell age and local density  $P(x, t)$ . This density dependence captures contact inhibition without imposing an explicit carrying capacity. Second, division and death are treated as distinct processes. This separation enables direct analysis of how ageing and division timing independently influence population dynamics.

We analyse five model cases (Table 1): constant rates (age-homogeneous), exponential decay (early division), and gamma-type profiles (maturation delay). These forms are chosen for analytical tractability and biological relevance. Each case is studied in both non-spatial ( $\kappa = 0$ ) and spatial ( $\kappa > 0$ ) settings.

TABLE 1  
Model cases studied in both non-spatial and spatial settings

Case	$\mu(a, P)$	$\beta(a, P)$
1	$\mu$	$\beta(1 - P)$
2	$\mu$	$\beta e^{-\alpha a}(1 - P)$
3	$\mu$	$\beta a e^{-\alpha a}(1 - P)$
4	$\mu P$	$\beta a e^{-\alpha a}(1 - P)$
5	$(\mu - \gamma a e^{-\alpha a})P$	$\beta a e^{-\alpha a}(1 - P)$

**2.1. Integro–differential reduction.** We now derive an integro–differential reduction of the age-structured system (2.2)–(2.3).

Integrating Equation (2.2) with respect to age, and assuming  $u(a, x, t) \rightarrow 0$  as  $a \rightarrow \infty$ , we obtain the population balance

$$(2.4) \quad \partial_t P = \kappa \Delta P(x, t) + B(x, t) - \int_0^\infty [\mu(a, P(x, t)) + \beta(a, P(x, t))] u(a, x, t) da,$$

where  $B(x, t) = u(0, x, t)$  is given by the renewal condition (2.3). When division and death rates depend only on the total population, the system closes in terms of  $P(x, t)$  alone; see Lemma 2.1 (proof in Appendix A). This corresponds to logistic-type dynamics (cf. Case 1).

LEMMA 2.1. *Suppose the division and death rates depend only on total density, i.e.  $\mu(a, P) = \mu(P)$  and  $\beta(a, P) = \beta(P)$ , with  $\mu, \beta \geq 0$  and continuous. Under the renewal condition (2.3), the total population  $P(x, t) = \int_0^\infty u(a, x, t) da$  satisfies the reaction-diffusion equation*

$$(2.5) \quad \partial_t P = \kappa \Delta P + [\beta(P) - \mu(P)] P.$$

More generally, for affine feedback  $\beta(P) = \beta_0 - \beta_1 P$  and  $\mu(P) = \mu_0 + \mu_1 P$ ,

$$(2.6) \quad \partial_t P = \kappa \Delta P + [(\beta_0 - \mu_0) - (\beta_1 + \mu_1)P] P,$$

where the linear growth rate is  $r = \beta_0 - \mu_0$  and the carrying capacity is  $K = (\beta_0 - \mu_0)/(\beta_1 + \mu_1)$ . Hence  $K > 0$  requires  $\beta_0 > \mu_0$  and  $\beta_1 + \mu_1 > 0$ .

For age-dependent rates, we introduce age-weighted moments that mirror the division kernel structures. For any fixed decay parameter  $\alpha > 0$ , define

$$(2.7) \quad C(x, t; \alpha) = \int_0^\infty e^{-\alpha a} u(a, x, t) da, \quad D(x, t; \alpha) = \int_0^\infty a e^{-\alpha a} u(a, x, t) da.$$

Multiplying Equation (2.2) by  $e^{-\alpha a}$  and integrating by parts with respect to  $a$  gives

$$(2.8) \quad \begin{aligned} \partial_t C &= \kappa \Delta C(x, t; \alpha) + B(x, t) - \alpha C(x, t; \alpha) \\ &\quad - \int_0^\infty [\mu(a, P(x, t)) + \beta(a, P(x, t))] e^{-\alpha a} u(a, x, t) da. \end{aligned}$$

Similarly, multiplying Equation (2.2) by  $a e^{-\alpha a}$  and integrating gives

$$(2.9) \quad \begin{aligned} \partial_t D &= \kappa \Delta D(x, t; \alpha) + C(x, t; \alpha) - \alpha D(x, t; \alpha) \\ &\quad - \int_0^\infty [\mu(a, P(x, t)) + \beta(a, P(x, t))] a e^{-\alpha a} u(a, x, t) da. \end{aligned}$$

These moments also appear directly in the boundary renewal term, which becomes case-dependent:

$$(2.10) \quad B(x, t) = \begin{cases} 2\beta(1 - P(x, t)) P(x, t), & \text{Case 1,} \\ 2\beta(1 - P(x, t)) C(x, t; \alpha), & \text{Case 2,} \\ 2\beta(1 - P(x, t)) D(x, t; \alpha), & \text{Cases 3–5.} \end{cases}$$

To express the integral loss terms in Equation (2.8) and Equation (2.9), i.e.,  $\int_0^\infty [\mu(a, P(x, t)) + \beta(a, P(x, t))] e^{-\alpha a} u(a, x, t) da$  and  $\int_0^\infty [\mu(a, P(x, t)) + \beta(a, P(x, t))] a e^{-\alpha a} u(a, x, t) da$ , we define higher-order moments. For any constant decay parameter  $\alpha > 0$ , define

$$(2.11) \quad \begin{aligned} I_0(t, x; \alpha) &= \int_0^\infty e^{-2\alpha a} u(a, x, t) da, & I_1(t, x; \alpha) &= \int_0^\infty a e^{-2\alpha a} u(a, x, t) da, \\ I_2(t, x; \alpha) &= \int_0^\infty a^2 e^{-2\alpha a} u(a, x, t) da. \end{aligned}$$

The evolution of  $(P, C, D)$  involves these higher moments, so the system does not close. We use positivity constraints and integral inequalities to bound  $I_k$  and derive population thresholds. Equations (2.4), (2.8), and (2.9), together with definitions (2.11) and case-specific  $B(x, t)$  in Equation (2.10), constitute the reduced integro–differential system.

**2.2. Population persistence: survival conditions and bounds on population size.** We assume a well-mixed system and determine when populations sustain positive steady states and derive upper bounds on equilibrium size.

The well-mixed system ( $\kappa = 0$ ) reduces to a transport-renewal model,

$$(2.12) \quad \begin{aligned} \frac{\partial u}{\partial t} + \frac{\partial u}{\partial a} &= -[\mu(a, P(t)) + \beta(a, P(t))] u(a, t), \\ u(0, t) &= B(t) = 2 \int_0^\infty \beta(a, P(t)) u(a, t) da, \\ P(t) &= \int_0^\infty u(a, t) da. \end{aligned}$$

If  $P(0) \leq 1$  then the total population  $P(t) \in [0, 1], \forall t$  by construction. This system admits an explicit solution via characteristics,

$$(2.13) \quad u(a, t) = \begin{cases} u_0(a-t) S(a-t, a, t; P), & a > t, \\ B(t-a) S(0, a, t-a; P), & 0 \leq a \leq t, \end{cases}$$

where the survival probability from age  $a_0$  to  $a$  (i.e., the probability that a cell neither dies nor divides during this interval) is given by

$$(2.14) \quad S(a_0, a, t; P) = \exp \left( - \int_{a_0}^a [\mu(a', P(a' - a_0 + t)) + \beta(a', P(a' - a_0 + t))] da' \right).$$

In the long-time limit, we assume convergence to a steady state,

$$(2.15) \quad u(a, t) \rightarrow F(a), \quad P(t) \rightarrow \bar{P},$$

where  $\bar{P}$  is the total population at equilibrium. The steady-state distribution satisfies

$$(2.16) \quad F'(a) = -[\mu(a, \bar{P}) + \beta(a, \bar{P})] F(a),$$

with  $F(0) = 2 \int_0^\infty \beta(a, \bar{P}) F(a) da$  and  $\bar{P} = \int_0^\infty F(a) da$ . We define the steady-state survival function

$$(2.17) \quad S(a, \bar{P}) = \exp \left( - \int_0^a [\mu(a', \bar{P}) + \beta(a', \bar{P})] da' \right),$$

so that the age distribution can be expressed explicitly as

$$(2.18) \quad F(a) = F(0) S(a, \bar{P}).$$

Substituting Equation (2.18) into the boundary condition (2.16) yields the integral constraint

$$(2.19) \quad 1 = 2 \int_0^\infty \beta(a, \bar{P}) S(a, \bar{P}) da.$$

This equation determines the possible steady states  $\bar{P}$ . A positive solution  $\bar{P} > 0$  indicates a viable, persistent population. Our moment reduction approach leads to explicit upper bounds  $P_c$ , derived case by case below, such that any steady state satisfies  $\bar{P} \leq P_c$ . These bounds hold under the assumptions that  $\beta(a, P)$  is non-increasing in  $P$ ,  $\mu(a, P)$  is non-decreasing in  $P$ , and the relevant moments  $C, D, I_k$  are finite.

*Case 1: Age-homogeneous dynamics.* When division and death rates are independent of age, all cells share the same survival probability regardless of time since division. We assume that

$$\mu(a, P) = \mu, \quad \beta(a, P) = \beta(1 - P),$$

with constants  $\mu > 0, \beta > 0$ , where the term  $\beta(1 - P)$  models contact inhibition: division potential decreases with density. Constant  $\mu$  implies death rate is the same at all densities.

The governing Equation (2.4) reduces to logistic growth (Lemma 2.1):

$$P'(t) = (\beta - \mu) P(t) \left( 1 - \frac{P(t)}{K} \right), \quad K = \frac{\beta - \mu}{\beta}.$$

Survival requires  $\beta > \mu$ ; otherwise  $P \equiv 0$  is the only steady state. When  $\beta > \mu$ , the unique positive equilibrium is

$$(2.20) \quad P_c = 1 - \frac{\mu}{\beta},$$

representing the classical logistic balance between proliferation and mortality.

*Case 2: Early-division bias.* When cells have short cell cycle times (e.g., embryonic stem cells or intestinal epithelial cells), division events occur predominantly shortly after the previous division. We therefore assume that

$$(2.21) \quad \mu(a, P) = \mu, \quad \beta(a, P) = \beta e^{-\alpha a} (1 - P),$$

with constants  $\mu, \beta, \alpha > 0$ . The parameter  $\alpha$  controls the decline in division rate and favours division at younger ages. The contact inhibition factor  $(1 - P)$  limits division at high density. Inserting these rates into the main PDE, Equation (2.2), and using the model reduction outlined in Section 2.1 yields a reduced moment system in the variables  $(P, C, I_0)$ ,

$$(2.22) \quad \begin{aligned} P'(t) &= -\mu P(t) + \beta(1 - P(t))C(t), \\ C'(t) &= -(\mu + \alpha)C(t) + \beta(1 - P(t))(2C(t) - I_0(t)). \end{aligned}$$

At steady state, algebraic relations between  $\bar{P}$ ,  $\bar{C}$ , and  $I_0$  with the constraint  $\bar{I}_0 \geq 0$  yields the survival condition  $2\beta > \mu + \alpha$ . Any positive steady state satisfies

$$(2.23) \quad P_c = 1 - \frac{\mu + \alpha}{2\beta}.$$

Compared to Case 1, the survival condition reflects the combined effects of mortality ( $\mu$ ) and age-related decline in division rates ( $\alpha$ ).

*Case 3: Maturation delay.* When cells require time to pass cell-cycle checkpoints (G1/S/G2/M) before dividing, division potential is low immediately after division and peaks at intermediate ages. We therefore assume that

$$\mu(a, P) = \mu, \quad \beta(a, P) = \beta a e^{-\alpha a} (1 - P),$$

with constants  $\mu, \beta, \alpha > 0$ . The division rate follows a gamma-type profile, which peaks at age  $a = 1/\alpha$ . Inserting these rates into Equation (2.2) and using the reduction framework (Section 2.1) yields a coupled moment system in the variables  $(P, C, D, I_1, I_2)$ ,

$$(2.24) \quad \begin{aligned} P'(t) &= -\mu P(t) + \beta(1 - P(t))D(t), \\ C'(t) &= -(\mu + \alpha)C(t) + \beta(1 - P(t))(2D(t) - I_1(t)), \\ D'(t) &= -(\mu + \alpha)D(t) + C(t) - \beta(1 - P(t))I_2(t). \end{aligned}$$

Solving this system at steady state, and imposing non-negativity of  $(I_1, I_2)$  yields the survival condition  $2\beta > (\mu + \alpha)^2$ . Any positive steady state satisfies

$$(2.25) \quad P_c = 1 - \frac{(\mu + \alpha)^2}{2\beta}.$$

The quadratic penalty reflects a compounded cost: cells must survive both background mortality ( $\mu$ ) and the period of low division probability before reaching peak fertility at age  $1/\alpha$ .

*Cases 4 and 5: Maturation delay with density-dependent death rate.* When cell death is driven by crowding rather than intrinsic processes, death rate scales with population density. We combine density-dependent death with the gamma-type division kernel from Case 3. In Case 4, we assume  $\mu(a, P) = \mu P$ . Using the reduction framework (Section 2.1) yields coupled moment equations in  $(P, C, D, I_1, I_2)$  analogous to those in Case 3. Again solving at steady state and assuming non-negativity of the higher moments yields a survival condition  $2\beta > \alpha^2$ , and the population bound becomes

$$(2.26) \quad P_c = \frac{-(\alpha\mu + \beta) + \sqrt{(\alpha\mu + \beta)^2 - \mu^2(\alpha^2 - 2\beta)}}{\mu^2}.$$

Case 5 extends this by incorporating age-dependent mortality. We assume  $\mu(a, P) = (\gamma - \mu a e^{-\alpha a})P$ , which captures elevated death rates at birth, a decline during maturation, and a subsequent rise with senescence. Despite this added complexity, the survival condition remains  $2\beta > \alpha^2$ , and the steady-state population is bounded above,

$$(2.27) \quad \bar{P} \leq \min(P_c, \beta/(\gamma + \beta)),$$

where  $P_c$  is given by Equation (2.26). The second constraint arises from moment sign requirements; for moderate  $\gamma$ , the first term is the relevant upper bound (see Supplementary Materials, Section 3.3).

The critical shift from Cases 1–3 is that the *survival condition* now depends only on the division kernel parameters  $(\beta, \alpha)$ , not on the death rate  $\mu$ . At low density ( $P \rightarrow 0$ ), density-dependent death terms vanish, so persistence is determined solely by the low-density division potential  $\beta(a, 0)$ . However, the equilibrium population level  $P_c$  does depend on  $\mu$ . This reflects how the death rates modulate the carrying capacity but not the survival condition.

These cases show a clear progression in how age structure constrains survival. Case 1 recovers the classical rule that net growth determines persistence. Case 2 imposes a linear penalty for early reproductive decline. Case 3 introduces a quadratic penalty that reflects the compounded challenge of surviving both a non-reproductive phase and background mortality. This progression quantifies the cost of delayed reproduction. In Cases 4–5, the survival condition depends only on division kernel shape, whereas death rate parameters affect the equilibrium bound  $P_c$ , and determine how large the population can be once it survives.

Figure 2 and Table 2 summarise these results. Numerical simulations confirm that steady-state populations respect their theoretical bounds  $P_c$ . In Case 1, solutions match the bound exactly because the moment system closes in  $P$ . Cases 2–3 track their respective bounds closely, while Cases 4–5 form bands beneath them. This banding stems from a fundamental difference in how mortality operates. In Cases 1–3, constant death rates affect growth at all densities. Both the survival condition and the equilibrium population density involve  $\mu$ , which sets a unique equilibrium for a given  $(\beta, \alpha, \mu)$ . In Cases 4–5, density-dependent death vanishes at low densities. Survival is  $\mu$ -independent, depending only on  $(\beta, \alpha)$ , but the bound  $P_c$  is  $\mu$ -dependent. This gives one degree of freedom: varying  $\mu$  while holding  $(\beta, \alpha)$  fixed produces one survival condition with different equilibria, hence the bands.

TABLE 2

Summary of non-spatial models: population bounds  $P_c$  (with  $\bar{P} \leq P_c$ ) and survival conditions admitting positive steady states.

Case	Upper bound $P_c$	Survival condition
1	$1 - \mu/\beta$	$\beta > \mu$
2	$1 - \frac{\mu + \alpha}{2\beta}$	$2\beta > \mu + \alpha$
3	$1 - \frac{(\mu + \alpha)^2}{2\beta}$	$2\beta > (\mu + \alpha)^2$
4	$\frac{-(\alpha\mu + \beta) + \sqrt{(\alpha\mu + \beta)^2 - \mu^2(\alpha^2 - 2\beta)}}{\mu^2}$	$2\beta > \alpha^2$
5	$\min\left(\frac{-(\alpha\mu + \beta) + \sqrt{(\alpha\mu + \beta)^2 - \mu^2(\alpha^2 - 2\beta)}}{\mu^2}, \frac{\beta}{\gamma + \beta}\right)$	$2\beta > \alpha^2, \mu > \gamma/\alpha e$

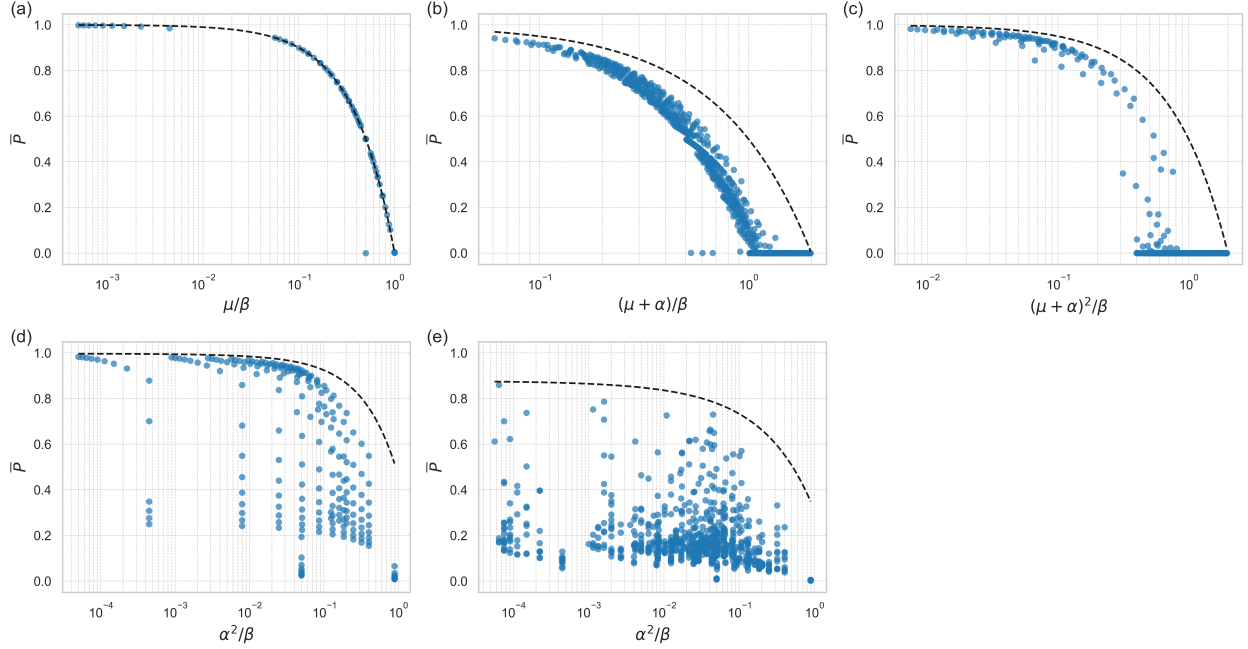


FIG. 2. Numerical steady-state population sizes  $\bar{P}$  plotted against threshold conditions (Table 2) for each non-spatial model (Cases 1–5). Dashed lines indicate the analytical upper bounds  $P_c$ . Each panel corresponds to a different model case: (a) Case 1; (b) Case 2; (c) Case 3; (d) Case 4; and (e) Case 5.

**3. Steady-state age distributions.** As established in Section 2.2, the steady-state age distribution (SSAD) takes the form  $F(a) = F(0)S(a; \bar{P})$ , where  $S(a; \bar{P})$  is the survival function and  $F(0)$  is determined by the renewal constraint (2.19). It describes the fraction of cells of age  $a$  in a population at equilibrium. Intuitively, it can be expressed as

$$(3.1) \quad F(a) = \text{renewal factor} \times \mathbb{P}(\text{cell survives beyond age } a) \\ \times \mathbb{P}(\text{cell does not divide by age } a),$$

which captures the balance between survival and renewal across ages. A useful summary measure is the mean population age,

$$(3.2) \quad \bar{a}_{\text{pop}} = \frac{\int_0^\infty aF(a)da}{\int_0^\infty F(a)da},$$

which quantifies the average time since last division for cells in the population at steady state.

Table 3 lists explicit formulae for  $F(a)$  across all five cases. The value of  $\bar{P}$  is found by solving the integral constraint (2.19) numerically. Once  $\bar{P}$  is known, either from this computation or from data, these formulae give  $F(a)$  directly without integrating the full PDE specified in Equation (2.12).

Figure 3 validates the analytical formulae. Panels (a–e) show numerical solutions (solid) match analytical predictions (dashed) across all cases. Panel (h) reveals a consistent pattern: mean division age  $\bar{a}_{\text{div}}$  falls below mean population age  $\bar{a}_{\text{pop}}$  in all cases. This occurs because divisions concentrate among cells in the reproductive window, while the population includes older, non-dividing survivors that persist in the tail and increase the mean age. The explicit SSADs therefore quantify how division timing shapes population structure. Age-independent rates (Cases 1–2) produce exponential-decay profiles because the division rates are constant across all ages. In contrast, gamma-type kernels (Cases 3–5) produce concave profiles near the origin. Newborn cells have a near-zero division probability, which causes them to accumulate into intermediate age classes before dividing.

**4. Cell-cycle-time distributions.** The cell-cycle-time distribution (CCTD) describes the timing of a cell's first division in a population at steady-state. It complements the steady-state age distribution (SSAD)

TABLE 3

Summary of steady-state age distributions  $F(a)$ . Cases 1-5 correspond to different division and death rate structures as defined in Table 1.

Case	$F(0)$	$F(a) = F(0) e^{-\int_0^a h(a') da'}$
1	$2\beta(1 - \bar{P})\bar{P}$	$F(0) e^{-\mu a - \beta a(1 - \bar{P})}$
2	$2\beta(1 - \bar{P})\bar{C}$	$F(0) e^{-\mu a - \frac{\beta(1 - \bar{P})}{\alpha}(1 - e^{-\alpha a})}$
3	$2\beta(1 - \bar{P})\bar{D}$	$F(0) e^{-\mu a - \frac{\beta(1 - \bar{P})}{\alpha^2}[1 - e^{-\alpha a}(1 + \alpha a)]}$
4	$2\beta(1 - \bar{P})\bar{D}$	$F(0) e^{-\mu a \bar{P} - \frac{\beta(1 - \bar{P})}{\alpha^2}[1 - e^{-\alpha a}(1 + \alpha a)]}$
5	$2\beta(1 - \bar{P})\bar{D}$	$F(0) e^{-\mu a \bar{P} + \frac{\gamma \bar{P}}{\alpha^2}[1 - e^{-\alpha a}(1 + \alpha a)] - \frac{\beta(1 - \bar{P})}{\alpha^2}[1 - e^{-\alpha a}(1 + \alpha a)]}$

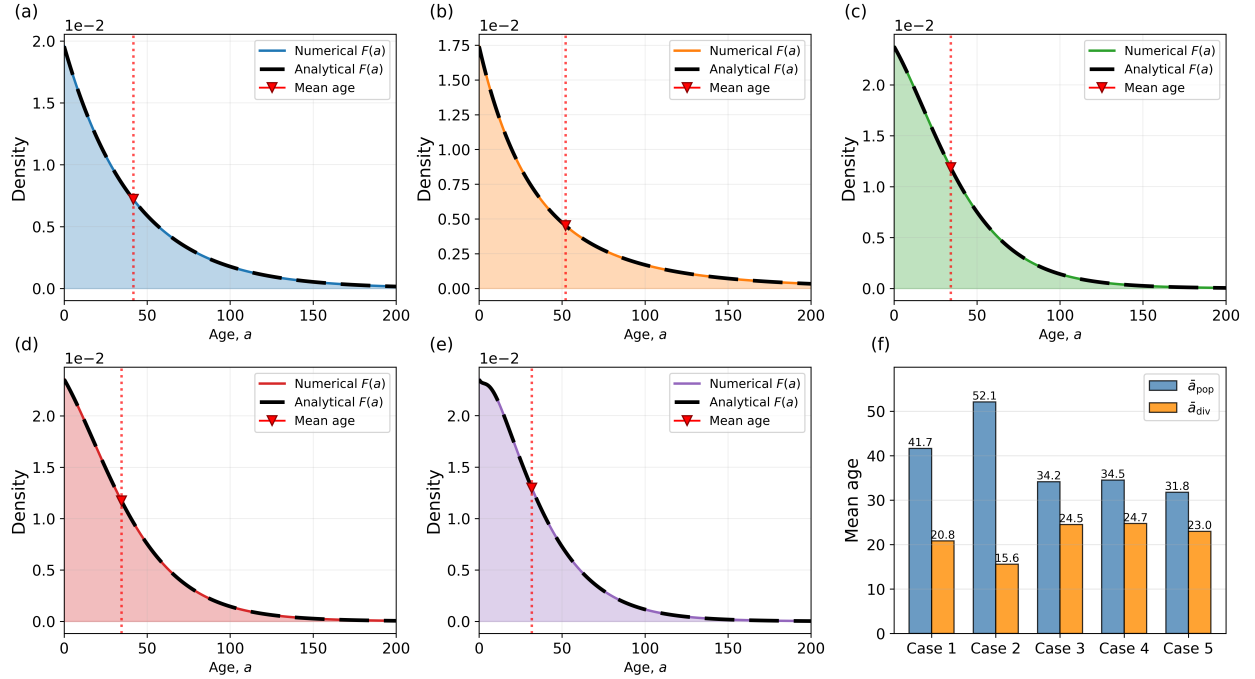


FIG. 3. Steady-state age distributions across five model cases with different division and death structures. Panels (a)-(e) show steady-state distributions  $F(a)$  for Cases 1-5: numerical solutions (coloured lines with shading) compared to analytical (black dashed lines). Red triangles mark the mean population age for each case. Panel (f) compares mean population age  $\bar{a}_{\text{pop}}$  and mean division age  $\bar{a}_{\text{div}}$  across all cases.

$F(a)$ , which describes population structure. Both derive from the survival probability  $S(a, \bar{P})$  (2.17), but represent different biological quantities. The CCTD can be interpreted heuristically as

$$(4.1) \quad f(a) = \text{division rate} \times \mathbb{P}(\text{cell survives beyond age } a) \\ \times \mathbb{P}(\text{cell does not divide by age } a),$$

which expresses the probability that a cell divides at age  $a$ . We formalise this by defining the unnormalised cell division density as  $\tilde{f}(a) = \beta(a, \bar{P})S(a, \bar{P})$ . This represents the density of cells undergoing their first division at age  $a$ , given by the fraction of survivors  $S(a, \bar{P})$  (cells that have survived without dying or dividing until age  $a$ ) multiplied by their instantaneous division rate  $\beta(a, \bar{P})$ . The normalised CCTD is then

$$(4.2) \quad f(a) = \frac{\beta(a, \bar{P})S(a, \bar{P})}{\int_0^\infty \beta(a', \bar{P})S(a', \bar{P}) da'}$$

which ensures  $\int_0^\infty f(a) da = 1$ . Using the SSAD  $F(a) = F(0)S(a, \bar{P})$ , the CCTD relates directly to the population structure:

$$(4.3) \quad f(a) = \frac{\beta(a, \bar{P})F(a)}{\int_0^\infty \beta(a', \bar{P})F(a') da'} = \frac{2\beta(a, \bar{P})F(a)}{F(0)},$$

where the renewal condition  $F(0) = 2 \int_0^\infty \beta(a, \bar{P})F(a) da$  gives the final form. Thus,  $f(a)$  is the division-weighted SSAD. The SSAD  $F(a)$  includes all cells, while the CCTD  $f(a)$  conditions on those that successfully divide.

A useful summary statistic is the mean division age defined by

$$(4.4) \quad \bar{a}_{\text{div}} = \int_0^\infty af(a) da,$$

which quantifies the expected timing of division events in the population.

The explicit forms of the CCTD for each case are given in Table 4; Cases 1–2 produce exponential-like profiles, while Cases 3–5 yield gamma-type distributions with delayed peaks. These formulae provide a direct link to experiments. One can fit them to lineage-tracing data to either infer the underlying division kernel shape or, if the kernel form is known, to estimate specific parameters like the peak division age ( $\alpha^{-1}$ ) and the maximum division rate ( $\beta$ ). This enables quantitative prediction of how division timing shapes population dynamics without conducting extensive numerical simulations. We first validate these expressions against numerical solutions (Fig. 4) and then demonstrate their application to experimental data (Fig. 5).

TABLE 4

*Cell-cycle-time distributions (CCTDs) for each model case. The distribution is given by  $f(a) = \beta(a, \bar{P})S(a, \bar{P})/Z$ , where  $Z$  is the normalization constant. The survival function is  $S(a, \bar{P}) = \exp(-\int_0^a h(a') da')$  with the removal rate  $h(a) = \mu(a, \bar{P}) + \beta(a, \bar{P})$ .*

Case	CCTD $f(a)$
1	$\beta(a, \bar{P}) e^{-(\mu+\beta(1-\bar{P}))a}$
2	$\beta(a, \bar{P}) e^{-\mu a - \frac{\beta(1-\bar{P})}{\alpha} [1-e^{-\alpha a}]}$
3	$\beta(a, \bar{P}) e^{-\mu a - \frac{\beta(1-\bar{P})}{\alpha^2} [1-e^{-\alpha a}(1+\alpha a)]}$
4	$\beta(a, \bar{P}) e^{-\mu a \bar{P} - \frac{\beta(1-\bar{P})}{\alpha^2} [1-e^{-\alpha a}(1+\alpha a)]}$
5	$\beta(a, \bar{P}) e^{-\mu a \bar{P} + \frac{\gamma \bar{P}}{\alpha^2} [1-e^{-\alpha a}(1+\alpha a)] - \frac{\beta(1-\bar{P})}{\alpha^2} [1-e^{-\alpha a}(1+\alpha a)]}$

Figure 4 illustrates how the CCTD expressions translate into observable cell division-timing patterns. Cases 1–2 concentrate divisions at young ages. The exponential form in Case 1 ( $k = 1.0$ ) reflects memoryless division timing, where cells have a constant division rate regardless of age, consistent with classical birth-death models. In Case 2 ( $k = 0.95$ ), division potential decreases exponentially with age, producing a hypoexponential distribution that shifts divisions to even earlier ages. This captures fast-cycling regimes where many cells divide soon after birth. In contrast, Cases 3–5 incorporate gamma-type division kernels  $\beta(a, \bar{P}) \propto a e^{-\alpha a}$ , which model a maturation delay and produce the bell-shaped CCTDs observed in lineage-tracing data [5, 24]. This captures the more realistic scenario where newly divided cells require time to prepare for the next division cycle. The peak location is set by  $a \approx 1/\alpha$ , while the distribution height and width are determined by  $\beta$  and the death rate  $\mu$ . All cases exhibit an exponential tail  $\sim e^{-\mu(a, \bar{P})}$ . Panel (f) overlays all normalised cases, showing the ordering implied by their means: exponential-decay division rates (Case 2) yield the lowest mean division age (15.6), followed by constant rates (Case 1, 20.8), then gamma-type cases (3–5) with later peaks and higher mean ages (23–25).

We fitted the analytical CCTD for Case 3 to lineage data from cells under control (DMSO) and drug-perturbed conditions (Fig. 5(a)–(c)). CHX (cycloheximide) is a protein synthesis inhibitor that lengthens the G1 phase, and erlotinib (ERL) is an EGFR inhibitor that extends all cycle phases. Case 3 was selected because its gamma-type division rate is the simplest form that produces the unimodal CCTD observed experimentally. The minimum cell-cycle time  $a_0$  was set to the 10th percentile of the data, fixing the left-hand support of the distribution. For each  $\alpha$  in a plausible range, we estimated  $(\beta, \mu)$  by minimising a

combined loss: the  $L^2$  difference between model and empirical cumulative distribution functions (CDFs), plus a weighting on tail survival probabilities to ensure accurate long-time behaviour. The survival condition  $2\beta > (\mu + \alpha)^2$  was enforced via quadratic penalty. The fitted parameters  $(\beta, \alpha, \mu)$  reflect the expected mechanisms: CHX and erlotinib reduce the division rate ( $\beta$ ) and increase the maturation timescale ( $1/\alpha$ ) compared to the DMSO control. Full fitting details and code are provided in the Supplementary Materials.

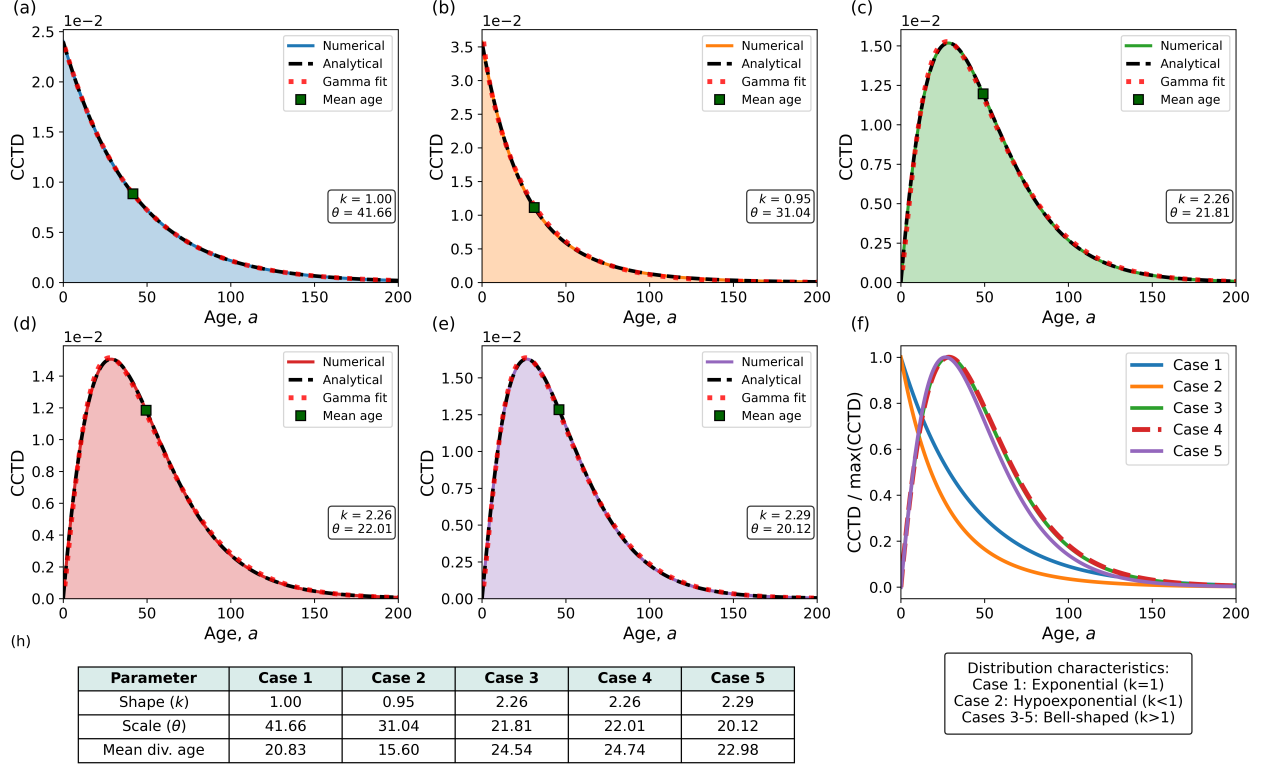


FIG. 4. Cell-cycle-time distributions across five model cases. Panels (a–e) show numerical CCTDs (solid) with fitted gamma distributions (dashed) for Cases 1–5; the fitted shape  $k$  and scale  $\theta$  parameters are indicated. Squares mark mean division ages. Panel (f) overlays all cases after normalisation to isolate shape differences: exponential (Case 1,  $k = 1$ ), hypoexponential (Case 2,  $k < 1$ ), and bell-shaped (Cases 3–5,  $k > 1$ ). Panel (h) summarises the fitted gamma parameters and mean division ages.

**5. Travelling waves and invasion thresholds.** We now examine travelling-wave solutions of the spatial ( $\kappa > 0$ ) models to assess how age structure modifies invasion speed. Classical Fisher–KPP theory predicts a single wave speed determined by the net growth rate. In the context of age-structured models, two distinct linear predictions emerge. The first,  $c_{\text{lin}}$ , arises from the moment-system approximation and coincides with the Fisher–KPP prediction. The second,  $c_{\text{min}}$ , obtained from the age-structured formulation, is systematically smaller. This discrepancy arises because the moment-system linearisation assumes uniform decay across all ages at the wave front, whereas the age-structured model preserves differential decay where younger cells dominate the front, and their lower division potential slows invasion. Moreover, the condition for a positive wave speed exactly matches the non-spatial survival threshold, linking persistence and invasion within a unified framework.

**5.1. Moment-system linearisation and the speed  $c_{\text{lin}}$ .** We seek solutions of the form

$$(5.1) \quad u(a, x, t) = \phi(a, z),$$

with  $z = x - ct$  and  $c > 0$ , representing a front propagating at constant speed  $c$ . We apply the travelling wave ansatz (5.1) to the reduced integro-differential system (2.4)–(2.11), expressing the population moments

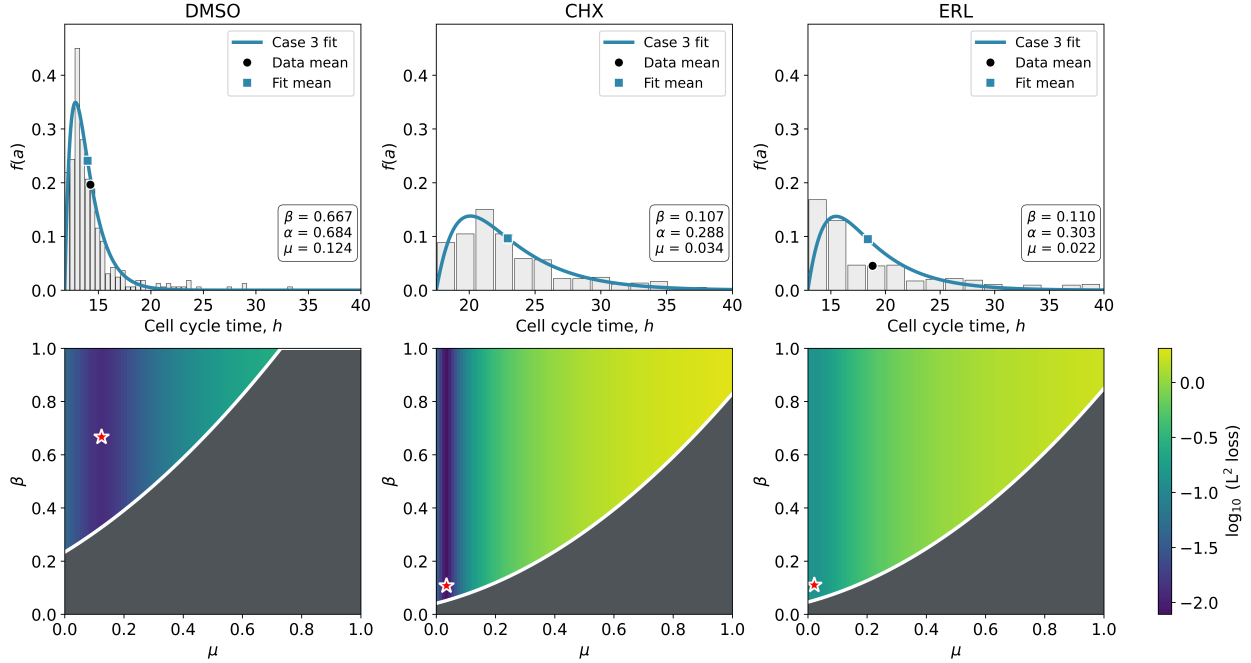


FIG. 5. Experimental cell-cycle time distributions with Case 3 distributions and gamma fits. Panels (a–c) show CCTDs under DMSO (vehicle control), cycloheximide (CHX), and erlotinib (ERL). Data are plotted with the Case 3 analytical CCTD fit (solid) and a gamma distribution fit (dashed). Insets report the fitted  $(\beta, \alpha, \mu)$ ; squares mark mean division age. Panels (d–f) show the corresponding loss landscapes in  $(\mu, \beta)$  at the fitted  $\alpha$  on a shared colour scale: the white curve is the constraint boundary  $\beta = \frac{1}{2}(\mu + \alpha)^2$  (i.e., parameter condition for survival per Table 2); the red star marks the optimum; infeasible regions are shaded. Axes are  $\mu \in [0, 1]$  and  $\beta \in [0, 1]$ . The infeasible region differs across panels because the feasibility boundary depends on the fitted  $\alpha$  for each dataset.

as functions of  $z$ ,

$$(5.2) \quad U(z) = \int_0^\infty \phi(a, z) da, \quad V(z; \alpha) = \int_0^\infty e^{-\alpha a} \phi(a, z) da,$$

$$(5.3) \quad W(z; \alpha) = \int_0^\infty a e^{-\alpha a} \phi(a, z) da, \quad \tilde{I}_k(z; \alpha) = \int_0^\infty a^k e^{-2\alpha a} \phi(a, z) da \quad \text{for } k = 0, 1, 2.$$

The parameter  $\alpha$  here represents the rate at which fertility declines with age in the division kernel. We linearise the resulting system about the extinction state where all moments vanish, i.e.  $U(z) = V(z; \alpha) = W(z; \alpha) = \tilde{I}_k(z; \alpha) = 0$  for  $k = 0, 1, 2$ . This is mathematically tractable and makes the specific biological assumption that all age classes vanish uniformly at the wave front. For each model case, this procedure yields an explicit expression for the wave speed, which we denote  $c_{\text{lin}}$ . For age-independent rates (Case 1), this gives the classical Fisher–KPP speed,  $c_{\text{lin}} = 2\sqrt{\kappa r}$  with  $r = \beta - \mu$ . For models with age structure,  $c_{\text{lin}}$  takes a more complex form but maintains the general structure  $2\sqrt{\kappa r_{\text{eff}}}$ , where  $r_{\text{eff}}$  is an effective low-density growth rate.

Table 5 summarises the wave speeds  $c_{\text{lin}}$  for Cases 1–5. Numerical simulations (Fig. 6) confirm that  $c_{\text{lin}}$  matches the observed invasion speed when division and death rates are age-independent (Case 1). For age-dependent rates, however,  $c_{\text{lin}}$  overestimates the observed speed because the age distribution at the wave front is not uniform. We derive the exact minimal speed  $c_{\text{min}}$  in the next section and show  $c_{\text{min}} \leq c_{\text{lin}}$  in all cases.

**5.2. Age-structured analysis and minimal wave speeds.** We apply the ansatz (5.1) to the governing PDE (2.2),

$$(5.4) \quad -c\phi_z + \phi_a = \kappa\phi_{zz} - [\mu(a, U(z)) + \beta(a, U(z))]\phi(a, z).$$

At the leading edge, where  $U(z) \rightarrow 0$ , the linearised system becomes

$$(5.5) \quad -c\phi_z + \phi_a = \kappa\phi_{zz} - [\mu(a, 0) + \beta(a, 0)]\phi(a, z),$$

with boundary condition

$$(5.6) \quad \phi(0, z) = 2 \int_0^\infty \beta(a, 0)\phi(a, z) da.$$

We seek solutions of the form  $\phi(a, z) = A(a)e^{-\lambda z}$ , where  $\lambda > 0$  determines the spatial decay rate. Substituting into (5.5) yields the age profile equation

$$(5.7) \quad A'(a) + [c\lambda - \kappa\lambda^2 + \mu(a, 0) + \beta(a, 0)] A(a) = 0,$$

with solution

$$(5.8) \quad A(a) = A(0) \exp \left[ - \int_0^a (c\lambda - \kappa\lambda^2 + \mu(s, 0) + \beta(s, 0)) ds \right].$$

Substituting (5.8) into (5.6) gives the dispersion relation

$$(5.9) \quad 1 = 2 \int_0^\infty \beta(a, 0) \exp \left[ - \int_0^a (c\lambda - \kappa\lambda^2 + \mu(s, 0) + \beta(s, 0)) ds \right] da.$$

The minimal wave speed  $c_{\min}$  is the infimum of  $c > 0$  over  $\lambda > 0$  satisfying (5.9). For tractable rate forms, (5.9) yields  $c_{\min}$  analytically. Otherwise, it reduces to a root-finding problem that is straightforward to compute numerically.

**5.3. Minimal wave speeds across model cases.** We now apply both linearisation approaches to Cases 1 and 5, deriving  $c_{\min}$  explicitly and showing that  $c_{\min} = c_{\text{lin}}$  for Case 1 but  $c_{\min} < c_{\text{lin}}$  for Case 5.

*Case 1: Age-homogeneous dynamics.* Consider the system (2.2)–(2.3) with

$$(5.10) \quad \mu(a, P) = \mu, \quad \beta(a, P) = \beta(1 - P).$$

This case serves as a benchmark where age structure decouples from invasion dynamics. We recall that the non-spatial survival condition is  $\beta > \mu$ .

Integrating the PDE (2.2) with respect to  $a$  and using the boundary condition  $u(0, x, t) = 2\beta(1 - P)P$  gives (Lemma 2.1)

$$(5.11) \quad \partial_t P = \kappa\Delta P + rP \left( 1 - \frac{P}{K} \right).$$

where  $r = \beta - \mu$  and  $K = (\beta - \mu)/\beta$ . Applying the travelling-wave ansatz  $P(x, t) = U(z)$ ,  $z = x - ct$ , and linearising about  $U = 0$  yields

$$(5.12) \quad \kappa\lambda^2 - c\lambda + (\beta - \mu) = 0.$$

This dispersion relation is identical to that obtained from the general formula (5.9) with  $\mu(a, 0) = \mu$  and  $\beta(a, 0) = \beta$ , confirming that the moment-system and age-structured linearisations agree. Hence

$$(5.13) \quad c_{\min} = c_{\text{lin}} = 2\sqrt{\kappa(\beta - \mu)}.$$

If  $\beta > \mu$  the population invades; otherwise the population goes extinct. This matches the non-spatial survival condition. Invasion speed depends solely on the net growth rate  $\beta - \mu$ , not age structure, linking persistence to spatial spread.

*Case 1b: Density-dependent death rate.* Consider a modification:  $\mu(a, P) = \mu P$  and  $\beta(a, P) = \beta(1 - P)$ . Lemma 2.1 applies, giving

$$(5.14) \quad \partial_t P = \kappa \Delta P + \beta P - (\beta + \mu) P^2.$$

This is again a Fisher–KPP-type equation with  $r = \beta$  and  $K = \beta/(\beta + \mu)$ . Since the division and death rates remain age-independent, we have  $c_{\min} = c_{\text{lin}}$ , with

$$(5.15) \quad c_{\min} = 2\sqrt{\kappa\beta}.$$

The key difference from Case 1 lies in how the death rate affects invasion. In Case 1, the death rate is independent of the density ( $\mu(a, P) = \mu$ ), reducing the net growth rate to  $r = \beta - \mu$ . In Case 1b, the death rate is density-dependent ( $\mu(a, P) = \mu P$ ) and vanishes at the wave front where  $P \rightarrow 0$ . The invasion speed is therefore governed by the division rate at low density, while the death rate regulates the carrying capacity behind the front.

*Case 5: Maturation delay with density-dependent death rate.* Consider

$$(5.16) \quad \mu(a, P) = (\mu - \gamma a e^{-\alpha a}) P, \quad \beta(a, P) = \beta a e^{-\alpha a} (1 - P),$$

where  $\mu > \gamma/(\alpha e)$  ensures the death rate remains positive, and the non-spatial threshold  $2\beta > \alpha^2$  guarantees population persistence.

Using the reduction framework of Section 2.1 and the ansatz (5.1), the moment system in travelling-wave coordinates becomes

$$(5.17) \quad \begin{aligned} -cU' &= \kappa U'' - \mu U^2 + \gamma U W + \beta(1 - U)W, \\ -cV' &= \kappa V'' - (\mu U + \alpha)V + \gamma U \tilde{I}_1 + \beta(1 - U)(2W - \tilde{I}_1), \\ -cW' &= \kappa W'' - (\mu U + \alpha)W + V + \gamma U \tilde{I}_2 - \beta(1 - U)\tilde{I}_2, \end{aligned}$$

where the  $\tilde{I}_k$  are defined as in (5.2). Linearising about  $(U, V, W) = (0, 0, 0)$ , where higher moments vanish because  $\phi(a, z) \rightarrow 0$ , yields

$$(5.18) \quad c_{\text{lin}} = 2\sqrt{\kappa \left( \sqrt{2\beta} - \alpha \right)}.$$

If  $2\beta > \alpha^2$ , which matches the condition for population persistence, the population invades; otherwise the population dies out. Unlike Case 1, however,  $c_{\text{lin}}$  provides only an upper bound. To obtain the exact minimal speed  $c_{\min}$ , we solve the dispersion relation (5.9). At the wave front where  $P \rightarrow 0$ ,  $\mu(a, 0) = 0$  and  $\beta(a, 0) = \beta a e^{-\alpha a}$ , giving

$$(5.19) \quad 1 = 2\beta \int_0^\infty a e^{-\alpha a} \exp \left[ -(c\lambda - \kappa\lambda^2)a - \frac{\beta}{\alpha^2} (1 - e^{-\alpha a}(1 + \alpha a)) \right] da.$$

The minimal speed  $c_{\min}$  is obtained by minimising  $c(\lambda)$  over  $\lambda > 0$  satisfying (5.19). Numerical solution (Fig. 6) confirms  $c_{\min} < c_{\text{lin}}$ .

In summary, the upper bound  $c_{\text{lin}}$  arises from linearising the moment system at the extinction state, assuming uniform decay across all age classes. The exact minimal speed  $c_{\min}$  accounts for the age-structured profile at the leading edge and satisfies  $c_{\min} \leq c_{\text{lin}}$ , with equality only when death and division rates are age-independent. We call invasion conditions the parameter conditions derived by requiring  $c_{\text{lin}} > 0$ , which coincide with the non-spatial survival thresholds for all cases (Table 2 (non-spatial) and Table 5 (spatial)). When invasion conditions hold, travelling waves exist with positive minimal speed; when they fail, populations cannot invade regardless of initial spatial configuration. And that is because population dies out.

In summary, the upper bound  $c_{\text{lin}}$  arises from linearising the moment system at the extinction state, assuming uniform decay across all age classes. The exact minimal speed  $c_{\min}$  accounts for the age-structured

TABLE 5

Summary of invasion speed bounds and conditions for the spatial models. The upper bound  $c_{\text{lin}}$  comes from moment-system linearisation, and the minimal speed  $c_{\text{min}}$  satisfies  $c_{\text{min}} \leq c_{\text{lin}}$ . Invasion conditions give the parameter regime where travelling waves exist (equivalently, where  $c_{\text{lin}} > 0$ ).

Spatial case	Invasion speed bound $c_{\text{lin}}$	Invasion condition
1	$2\sqrt{\kappa(\beta - \mu)}$	$\beta > \mu$
1b	$2\sqrt{\kappa\beta}$	$\beta > 0$
2	$2\sqrt{\kappa(2\beta - \mu - \alpha)}$	$2\beta > \mu + \alpha$
3	$2\sqrt{\kappa(\sqrt{2\beta} - \mu - \alpha)}$	$2\beta > (\mu + \alpha)^2$
4	$2\sqrt{\kappa(\sqrt{2\beta} - \alpha)}$	$2\beta > \alpha^2$
5	$2\sqrt{\kappa(\sqrt{2\beta} - \alpha)}$	$2\beta > \alpha^2$

profile at the leading edge and satisfies  $c_{\text{min}} \leq c_{\text{lin}}$ , with equality only when division and death rates are age-independent. The invasion conditions are parameter constraints derived by requiring  $c_{\text{lin}} > 0$  and coincide with the non-spatial survival thresholds for all cases (Table 2 and Table 5). When invasion conditions hold, travelling waves exist with positive minimal speed; when they fail, populations cannot invade regardless of initial spatial configuration, as the population dies out locally before spatial spread can occur.

Numerical solutions of the governing PDE (2.2) converge to travelling waves with speeds matching theoretical predictions (Fig. 6). For age-independent rates (Case 1),  $c_{\text{min}} = c_{\text{lin}}$ . For age-dependent rates (Cases 3, 5),  $c_{\text{min}} < c_{\text{lin}}$ . Figure 7 reveals the mechanism. The top row shows where cell division occurs spatially. In Case 1, division concentrates at the leading edge. In Cases 3 and 5, cell division concentrates slightly behind the leading edge. Consequently, peak division occurs not at the leading edge but at positions where cells have aged sufficiently to reach peak division rates. The bottom row shows death loss and division loss. In Case 1, high division rates at the front drive rapid invasion. In Cases 3 and 5, lower division rates at the front slow the wave.

The inequality  $c_{\text{min}} \leq c_{\text{lin}}$  quantifies how age structure affects invasion speed. The bound  $c_{\text{lin}}$  assumes all ages contribute equally at the wave front and yields a tractable expression that depends only on division and death rates at low density. The exact minimal speed  $c_{\text{min}}$  accounts for the age distribution at the leading edge but requires solving a dispersion relation numerically. Computing both quantities provides a diagnostic: if  $c_{\text{min}} \approx c_{\text{lin}}$ , age structure is negligible; if  $c_{\text{min}} \ll c_{\text{lin}}$ , age-structure substantially affects invasion speed.

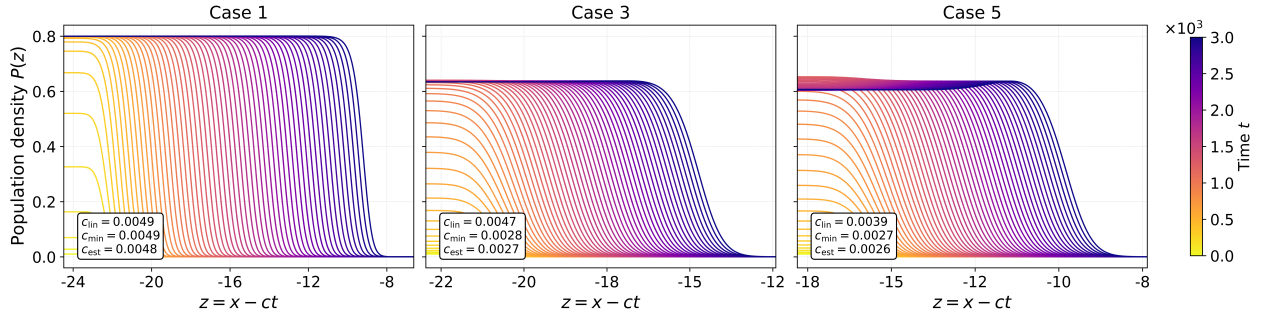


FIG. 6. Travelling wave profiles for different model cases. Each panel shows the evolution of the population density  $P(z)$  as a function of the travelling wave coordinate  $z = x - ct$ . The numerically estimated wave speed  $c_{\text{est}}$  approximates the theoretical minimal wave speed  $c_{\text{min}}$ . The wave speed predicted by the linear theory  $c_{\text{lin}}$  is also provided. Parameters:  $\alpha = 0.01$ ,  $\mu = 0.005$ ,  $\kappa = 3 \times 10^{-4}$ ;  $\beta$  satisfies  $\beta = r \times$  (invasion condition) with  $r = 5$  and invasion conditions from Table 2, which places each case at the same relative distance above its extinction threshold. Case 5 additionally requires  $\gamma < \mu\alpha\epsilon$  to ensure non-negative death rates. We set  $\gamma = 1 \times 10^{-4}$ .

**6. Discussion.** We developed an analytical framework for age-structured cell populations that separates division and death processes explicitly and reduces the governing transport-renewal PDE to a tractable

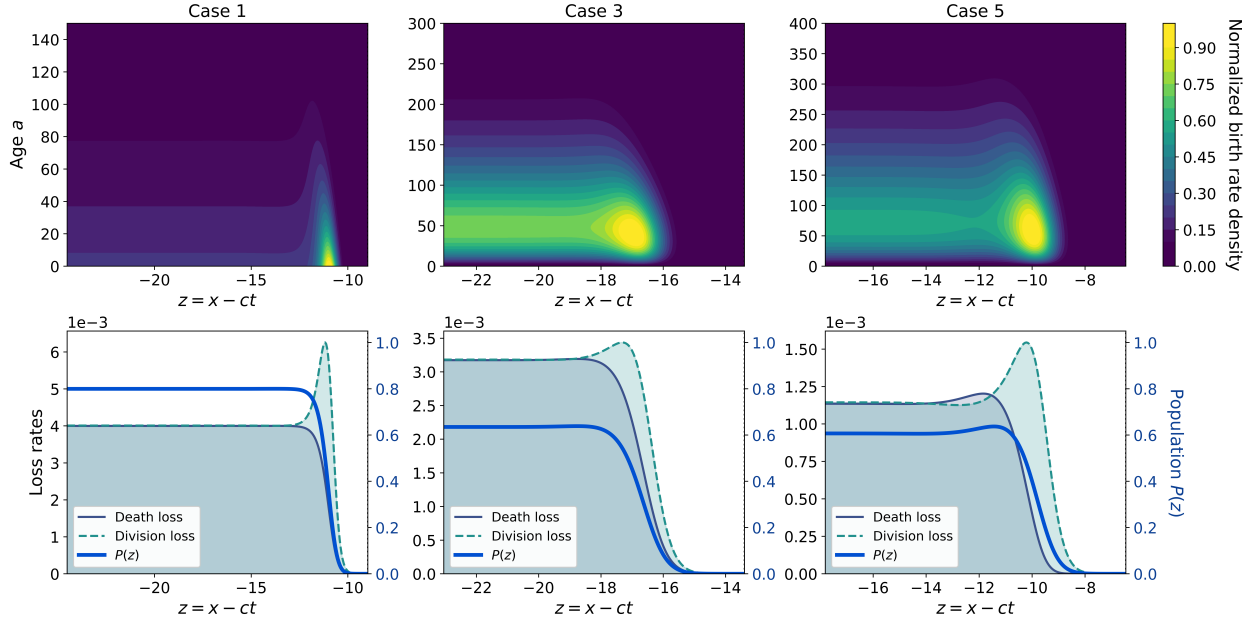


FIG. 7. Population structure and birth-death dynamics for different division kernels. Top row: normalised division rate density  $\beta(a, z)u(a, z)$  in the travelling wave frame, showing the spatial distribution of new cells across age classes. Bottom row: death and division loss rates (left axis) alongside total population density  $P(z)$  (right axis), illustrating the balance between losses (cell death and division) and population renewal (birth influx via daughter cells). Parameters are as in Figure 6.

integro-differential system. Using this reduction, we derived explicit expressions for the SSAD, the CCTD, and the invasion speeds, and achieved analytical tractability previously limited to homogeneous populations. A fundamental duality emerges: the condition for population persistence is identical to the condition for spatial invasion. If this condition fails, the population does not generate a front and declines to extinction. This correspondence holds across all model cases. Moreover, when the division and death rates are age-independent, the system reduces to a logistic or Fisher-KPP equation; when the rates depend explicitly on age, the same framework yields rigorous bounds, including the survival threshold  $P_c$ , the wave-speed upper bound  $c_{\text{lin}}$ , and the exact minimal speed  $c_{\text{min}}$ . The difference  $c_{\text{lin}} - c_{\text{min}}$  quantifies how the assumption of a uniform division rate across the cell population leads to an overestimation of the true invasion speed. In modelling applications such as wound healing or tumour invasion, models that neglect age-dependent division rates systematically overestimate the rate of spatial advance.

**Age structure changes the rules of population persistence.** We first examined the growth dynamics of populations without spatial structure. The framework yields explicit survival conditions (Table 2) confirmed by numerical simulations (Fig. 2). These conditions follow a systematic pattern. For age-independent dynamics (Case 1), population persistence requires only that the division rate exceeds the death rate ( $\beta > \mu$ ). When the division rate varies with age, stricter criteria emerge. An early-division bias, where division rate decays exponentially at rate  $\alpha$  (Case 2), requires  $2\beta > \mu + \alpha$ . A maturation delay, where division rate peaks at age  $\sim 1/\alpha$  (Case 3), requires  $2\beta > (\mu + \alpha)^2$ . Cases 4–5 represent a qualitatively different regime. When the death rate is density-dependent ( $\mu(a, P) = \mu P$ ) with a maturation delay in the division rate, the survival condition simplifies to  $2\beta > \alpha^2$ , which depends solely on the division rate. In these cases the division mechanism sets the survival condition, whereas the death rate determines only the equilibrium population size (see  $P_c$  in Table 2).

**Age structure at invasion fronts slows spatial spread.** Invasion speed depends on the division rate at low density. Case 1 illustrates the classical scenario where division rates are age-independent, so newborn cells at the leading edge divide at the same rate as older cells, and the wave propagates at the Fisher-KPP speed ( $c_{\text{min}} = c_{\text{lin}}$ ). In Cases 3 and 5, the leading edge is dominated by newborn cells with low division rates, whereas peak division rate occurs behind the front. This maturation delay explains why

$c_{\min} < c_{\text{lin}}$  in these cases. Cell populations that can divide soon after division (Cases 1–2) invade faster than those requiring maturation before division (Cases 3–5). Far behind the leading edge in all cases, the population reaches equilibrium where the division and death rates balance (Figure 7, bottom row), but this region does not drive front propagation.

**Explicit distributions link mechanism to data.** The framework yields explicit expressions for the SSAD and the CCTD (Tables 3, 4). These distributions follow from the same division and death rates but emphasise distinct features of the population. The SSAD describes the age profile of the entire population; the CCTD describes the timing of first divisions. Age-independent division rates produce exponential CCTDs. Gamma-type division rates produce bell-shaped CCTDs that peak at intermediate ages, matching the maturation delays observed in lineage data [5, 24]. The mean division age and the mean population age can be obtained from the CCTD and the SSAD, respectively. The mean division age systematically lies below the mean population age (Fig. 4 h) because cell divisions concentrate among younger cells, whereas the SSAD retains older cells that have neither died nor divided.

Experimental techniques such as fluorescent cell-cycle reporters [6] identify the current phase of an individual cell (G1/S/G2/M) but not the duration of that phase [25]. Lineage tracing quantifies cell-cycle time yet requires long-term tracking. The analytical CCTD provides a direct route from data to population-level parameters ( $\beta, \alpha, \mu$ ), as illustrated in Fig. 6 for drug treatments where fitted values fall near the theoretical survival thresholds. The same parameters determine the SSAD and predict persistence and invasion speed without live-cell imaging or simulation of the full PDE system. Earlier work established equivalence between multi-stage stochastic models and age-structured PDEs [7, 10]. Our explicit formulae extend that foundation and permit direct parameter inference from standard experimental measurements.

Our framework aggregates the cell-cycle phases into a single age variable, which provides analytical tractability but has limitations. It cannot resolve phase-specific regulation (e.g., G1 versus S/G2/M delays) or model heritable differences in division timing—the ‘two-clock’ problem in which biological and chronological age diverge [11]. Cells that cycle rapidly may be biologically older despite less chronological time elapsed, and this disparity affects population dynamics in ways our framework does not yet capture. Future work will extend the framework in two directions. First, multi-stage models could test whether the persistence and invasion principles persist under finer cell-cycle resolution. Second, allowing the rate of biological ageing to vary could reveal how internal clocks, distinct from chronological time, modulate population dynamics.

## Declarations

**Authorship and contributorship.** All authors have made substantial intellectual contributions to the study conception, execution, and design of the work. All authors have read and approved the final manuscript. Contributions were as follows: Conceptualisation: Stéphanie M. C. Abo, Ruth E. Baker; Methodology: Stéphanie M. C. Abo, Ruth E. Baker; Software: Stéphanie M. C. Abo; Formal analysis and investigation: Stéphanie M. C. Abo; Writing – original draft preparation: Stéphanie M. C. Abo; Writing – review and editing: Stéphanie M. C. Abo, Ruth E. Baker; Supervision: Ruth E. Baker; Funding acquisition: Ruth E. Baker.

**Funding.** Ruth E. Baker is supported by a grant from the Simons Foundation (MP-SIP-00001828).

**Acknowledgements.** We thank Christian A. Yates for sharing unpublished cell-cycle data originally collected by Richard L. Mort and Matthew J. Ford; Rachel N. Leander for providing access to the DMSO, CHX, and ERL datasets available at [https://github.com/rnleander/DDT\\_cell\\_cycle](https://github.com/rnleander/DDT_cell_cycle). We also thank Mike B. Giles for helpful discussions on the formulation and implementation of the numerical scheme.

For the purpose of open access, the authors have applied a CC BY public copyright licence to any author accepted manuscript arising from this submission.

**Conflicts of interest.** The authors declare there are no conflicts of interest.

**Consent for publication** All the authors approved the final version of the manuscript.

**Code availability.** All code used for the simulations and figure generation is publicly available on GitHub at <https://github.com/Stephanie-Abo/age-structured-invasion-dynamics.git>.

- [1] K. Aoki, Y. Kondo, N. Honda, T. Hiratsuka, R. E. Itoh, and M. Matsuda. Propagating wave of erk activation orients collective cell migration. *Developmental Cell*, 43(3):305–317, 2017.
- [2] M. A. Heinrich, R. Alert, J. M. LaChance, T. J. Zajdel, A. Košmrlj, and D. J. Cohen. Size-dependent patterns of cell proliferation and migration in freely-expanding epithelia. *eLife*, 9:e58945, 2020.
- [3] L. Donker, R. Houtekamer, M. Vliem, F. Sipieter, H. Canever, M. Gomez-Gonzalez, M. Bosch-Padros, W.-J. Pannekoek, X. Trepast, and N. Borghi. A mechanical g2 checkpoint controls epithelial cell division through e-cadherin-mediated regulation of wee1-cdk1. *Cell Reports*, 41(2), 2022.
- [4] C. Falcó, D. J. Cohen, J. A. Carrillo, and R. E. Baker. Quantifying tissue growth, shape and collision via continuum models and bayesian inference. *Journal of the Royal Society Interface*, 20(204):20230184, 2023.
- [5] J. A. Smith and L. Martin. Do cells cycle? *Proceedings of the National Academy of Sciences*, 70(4):1263–1267, 1973.
- [6] A. Sakaue-Sawano, H. Kurokawa, T. Morimura, A. Hanyu, H. Hama, H. Osawa, S. Kashiwagi, K. Fukami, T. Miyata, and H. Miyoshi. Visualizing spatiotemporal dynamics of multicellular cell-cycle progression. *Cell*, 132(3):487–498, 2008.
- [7] C. A. Yates, M. J. Ford, and R. L. Mort. A multi-stage representation of cell proliferation as a Markov process. *Bulletin of Mathematical Biology*, 79(12):2905–2928, 2017.
- [8] W. Jiang. Cell cycle checkpoints callout (layout). [BioRender template](#), 2025. Accessed: 2025-09-15.
- [9] Z. W. Jones, R. Leander, V. Quaranta, L. A. Harris, and D. R. Tyson. A drift-diffusion checkpoint model predicts a highly variable and growth-factor-sensitive portion of the cell cycle g1 phase. *PLOS ONE*, 13(2):1–20, 2018.
- [10] J. C. Kynaston, C. Guiver, and C. A. Yates. Equivalence framework for an age-structured multistage representation of the cell cycle. *Physical Review E*, 105(6):064411, 2022.
- [11] K. Öcal and M. P. H. Stumpf. The two-clock problem in population dynamics. *arXiv preprint*, 2025. arXiv:2504.20388.
- [12] H. Kang, S. Ruan, and X. Yu. Age-structured population dynamics with nonlocal diffusion. *Journal of Dynamics and Differential Equations*, 34(2):789–823, 2022.
- [13] K. Dietz. Introduction to mckendrick (1926) applications of mathematics to medical problems. In S. Kotz and N. L. Johnson, editors, *Breakthroughs in Statistics*, pages 17–57. Springer, New York, NY, 1997.
- [14] H. von Foerster. Some remarks on changing populations. In F. Stohman, editor, *The Kinetics of Cellular Proliferation*, pages 382–407. Grune and Stratton, 1959.
- [15] M. E. Gurtin and R. C. MacCamy. Some simple models for nonlinear age-dependent population dynamics. *Mathematical Biosciences*, 43(3–4):199–211, 1979.
- [16] M. E. Gurtin and R. C. MacCamy. Diffusion models for age-structured populations. *Mathematical Biosciences*, 54(1–2):49–59, 1981.
- [17] J. Al-Omari and S. A. Gourley. Monotone travelling fronts in an age-structured reaction-diffusion model of a single species. *Journal of Mathematical Biology*, 45(4):294–312, 2002.
- [18] S. A. Gourley. Linear stability of travelling fronts in an age-structured reaction–diffusion population model. *The Quarterly Journal of Mechanics and Applied Mathematics*, 58(2):257–268, 2005.
- [19] G. Li, M. Mei, and Y. S. Wong. Nonlinear stability of traveling wavefronts in an age-structured reaction-diffusion population model. *Mathematical Biosciences and Engineering*, 5(1):85–100, 2008.
- [20] M. Mei and Y. S. Wong. Novel stability results for traveling wavefronts in an age-structured reaction-diffusion equation. *Mathematical Biosciences and Engineering*, 6(4):743–752, 2009.
- [21] R. E. Nixon, H. M. Byrne, J. M. Pitt-Francis, and P. K. Maini. Characterising the behaviour of a structured pde model of the cell cycle in contrast to a corresponding ode system. *Bulletin of Mathematical Biology*, 87(7):93, 2025.
- [22] G. Pang and É. Pardoux. Functional law of large numbers and PDEs for epidemic models with infection-age dependent infectivity. *Applied Mathematics and Optimization*, 87(3):50, 2023.
- [23] G. Belluccini, M. López-García, G. Lythe, and C. Molina-París. Counting generations in birth and death processes with competing erlang and exponential waiting times. *Scientific Reports*, 12:11289, 2022.
- [24] R. Leander, E. J. Allen, S. P. Garbett, D. R. Tyson, and V. Quaranta. Derivation and experimental comparison of cell-division probability densities. *Journal of Theoretical Biology*, 359:129–135, 2014.
- [25] A. E. Eastman, X. Chen, X. Hu, A. A. Hartman, A. M. P. Morales, C. Yang, J. Lu, H. Y. Kueh, and S. Guo. Resolving cell cycle speed in one snapshot with a live-cell fluorescent reporter. *Cell Reports*, 31(12), 2020.

### Appendix A. Proof of Lemma 2.1.

*Proof.* Integrate (2.2) with respect to  $a$  with  $u(\infty, x, t) = 0$  to give

$$(A.1) \quad \partial_t P - u(0, x, t) = \kappa \Delta P - \int_0^\infty [\mu(P) + \beta(P)] u \, da.$$

Since  $\mu, \beta$  depend only on  $P$ ,  $\int_0^\infty [\mu(P) + \beta(P)] u \, da = [\mu(P) + \beta(P)] P$ . From (2.3),  $u(0, x, t) = 2\beta(P)P$ , and  $\int_0^\infty u \, da = P$ . Substitution yields (2.5).  $\square$

**Appendix B. Mathematical and biological background.** A fundamental constraint in cell proliferation is the need to complete a sequence of preparatory phases before division can occur. This introduces a delay between a cell’s birth (via division of a mother cell) and its ability to divide again. Experimentally observed division-time distributions are typically peaked and right-skewed, rather than exponential, reflecting this maturation delay. Classical models of population dynamics track total cell density and assume a constant division rate independent of time since the last division. This assumption yields exponentially distributed division times and has enabled major progress in understanding population-level phenomena but does not capture the time delay constraint. To incorporate this biological constraint, we introduce *cell age*—the time since the last division—as a measurable proxy for cell-cycle progression. The framework then tracks how the population’s age distribution shapes collective outcomes such as survival and spatial spread.

The dynamics are formalised by a PDE describing the cell density  $u(a, x, t)$  as a function of age  $a$ , spatial position  $x$ , and time  $t$ . The model incorporates four biological processes: random cell motion; cell ageing at unit rate (a newborn cell at time  $t$  reaches age  $a$  at time  $t + a$ ); death at rate  $\mu(a, P)$ , which may depend on both age (e.g., senescence) and local crowding  $P$ ; and division at rate  $\beta(a, P)$ , which typically increases with age (reflecting maturation) and decreases with crowding (reflecting contact inhibition). Each division event produces two daughter cells of age zero. This *age-structured population equation* provides a minimal framework linking single-cell dynamics to population-level behaviour. The key idea is that reproduction depends on the distribution of times since the last division, introducing a memory effect: the current division rate depends on the entire age structure, not only on total population size.

A central analytical challenge is the model’s circular dependency: newborn cells (age zero) arise only from older cells dividing, so the division rate at any moment depends on the current age structure. But the age structure itself depends on past division rates. When division and death rates depend on both age structure and density, this creates a feedback loop between population history and current growth. We address this by deriving a reduced system based on weighted integrals of the age distribution, including the total population density  $P(x, t)$  and related moments that summarise the population structure. This reduction preserves the essential influence of cell age and yields tractable equations. From these, we obtain explicit, testable expressions for population survival conditions, steady-state age distributions (the fraction of cells at each age in a population at steady-state), and cell-cycle-time distributions (the distribution of division times in a population at steady-state). These results enable parameter estimation directly from lineage-tracing data without requiring full numerical simulation of the PDE system.

We also analyse travelling-wave solutions that describe expanding fronts of cells invading unpopulated regions. A key question is how rapidly the population spreads into free space. Classical theory with exponential division times predicts a wave speed  $c_{\text{lin}} = 2\sqrt{\kappa r}$ , where  $\kappa$  is the random motility coefficient and  $r$  the net growth rate. In our age-structured framework, the actual speed  $c_{\text{min}}$  satisfies  $c_{\text{min}} \leq c_{\text{lin}}$ . The biological interpretation is that the cell cycle imposes a cost on spatial spread. Cells at the front of the wave are young and thus unlikely to divide immediately. Because local proliferation drives population invasion, this transient loss of reproductive potential reduces the growth rate at the wave front. As a result, we observe a slower invasion speed than predicted by memoryless models. This finding implies that classical, memoryless models systematically overestimate invasion rates when division potential is not homogeneous in a cell population.

### Appendix C. Further reading.

#### *Cell-cycle regulation and division timing.*

- [1] D. O. Morgan, *The Cell Cycle: Principles of Control*, New Science Press in association with Oxford University Press, London, 2007.
- [2] S. D. Cappell, M. Chung, A. Jaimovich, S. L. Spencer, and T. Meyer, Irreversible APC<sup>Cdh1</sup> inactivation underlies the point of no return for cell-cycle entry, *Cell*, 166 (2016), pp. 167–180.

- [3] V. K. Gupta and O. Chaudhuri, Mechanical regulation of cell-cycle progression and division, *Trends in Cell Biology*, 32 (2022), pp. 773–785.
- [4] J. J. Tyson and B. Novák, Models in biology: lessons from modeling regulation of the eukaryotic cell cycle, *BMC Biology*, 13 (2015), art. 46.

***Age-Structured Population Models and Spatial Dynamics.***

- [1] M. Iannelli and F. Milner, *The Basic Approach to Age-Structured Population Dynamics*, Lecture Notes on Mathematical Modelling in the Life Sciences, Springer, Dordrecht, 2017.
- [2] H. R. Thieme, *Mathematics in Population Biology*, Princeton Series in Theoretical and Computational Biology, Princeton University Press, Princeton, NJ, 2003.
- [3] J. A. J. Metz and O. Diekmann (eds.), *The Dynamics of Physiologically Structured Populations*, Lecture Notes in Biomathematics, vol. 68, Springer-Verlag, Berlin, 1986.
- [4] J. D. Murray, *Mathematical Biology. I: An Introduction*, 3rd ed., Interdisciplinary Applied Mathematics, vol. 17, Springer-Verlag, New York, 2002.
- [5] J. D. Murray, *Mathematical Biology. II: Spatial Models and Biomedical Applications*, 3rd ed., Interdisciplinary Applied Mathematics, vol. 18, Springer-Verlag, New York, 2003.
- [6] O. Diekmann, M. Gyllenberg, and J. A. J. Metz, Steady-state analysis of structured population models, *Theoretical Population Biology*, 63 (2003), pp. 309–338.